ACS OMEGA

http://pubs.acs.org/journal/acsodf

Article

Choice of Protein, Not Its Amyloid-Fold, Determines the Success of Amyloid-Based Scaffolds for Cartilage Tissue Regeneration

Maurice C.E. van Dalen, Marcel Karperien, Mireille M.A.E. Claessens, and Janine N. Post*

Cite This: https://doi.org/10.1021/acsomega.3c00151

Read Online

ACCESS | Metrics & More | Article Recommendations | Supporting Information

ABSTRACT: The formation of fibrocartilage during articular cartilage regeneration remains a clinical problem affecting adequate restoration of articular cartilage in joints. To stimulate chondrocytes to form articular cartilage, we investigated the use of amyloid fibril-based scaffolds. The proteins α-synuclein, β-lactoglobulin, and lysozyme were induced to self-assemble into amyloid fibrils and, during dialysis, formed micrometer scale amyloid networks that resemble the cartilage extracellular matrix. Our results show that lysozyme amyloid micronetworks supported chondrocyte viability and extracellular matrix deposition, while α-synuclein and β-lactoglobulin maintained cell viability. With this study, we not only confirm the possible use of amyloid materials for tissue regeneration but also demonstrate that the choice of protein, rather than its amyloid-fold per se, affects the cellular response and tissue formation.

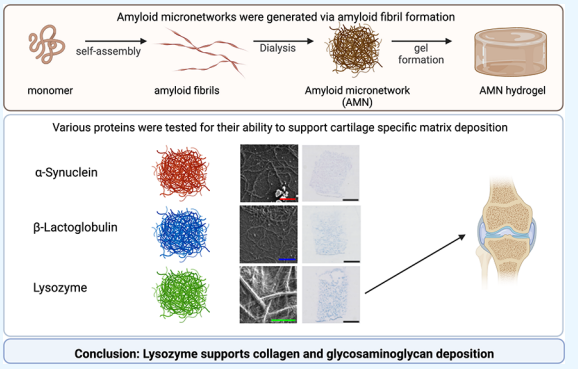

INTRODUCTION

Cartilage tissue regeneration remains a clinical and scientific challenge. Degenerative cartilage diseases, such as osteoarthritis, affect hyaline cartilage found in articulating joints.[1,2] The mechanical properties of this hydrogel-like tissue, in combination with a very low surface friction, make it difficult to engineer a material with similar properties for tissue replacement.[3] Enabling cells to regenerate lost cartilage tissue with the required local architecture and properties therefore seems a more viable approach. However, clinically used cell-based techniques are no guaranty for patient improvement, as newly formed tissue often includes fibrocartilage, which has inferior mechanical properties compared to native hyaline cartilage.[4,5] A biomimetic scaffold could improve the quality of regenerated cartilage.[3,6,7] Such a scaffold would reduce dedifferentiation associated with chondrocyte expansion, while incorporated cues could stimulate chondrocytes to regenerate hyaline cartilage.

Mimicking the extracellular matrix (ECM) of cartilage, which is built up for a large part by collagen type 2 bundles interconnected with proteoglycans, requires a scaffold material with similar properties. Amyloid materials resemble collagen, since both are composed of fibrils with a similar strength and Young's modulus.[8,9] Many proteins can be induced to adopt a cross β-sheet structure and assemble into amyloid fibrils that are micrometers in length and several nanometers in diameter. Furthermore, like collagen, the fibrils can be used for the formation of hydrogels.[9−14] Other properties of naturally occurring amyloid structures also support their possible use as scaffold material. Amyloid fibrils are used for protection of a cell's surroundings,[15] cell attachment,[16] and hormone storage and release.[17] Summarizing, hydrogels of amyloid fibrils resemble key characteristics of the ECM of cartilage.

Redifferention of chondrocytes can be achieved with hydrogels with a storage and loss modulus of ∼10 and 0.3 kPa or lower, respectively,[18] and values of the same order of magnitude can be obtained for amyloid hydrogels by selection and optimization of the gelation conditions.[19−21] In a previous work, we showed that amyloid networks of lysozyme fibril have a viscoelasticity relevant to tissue engineering and other biomedical applications.[22] We hypothesized that networks of amyloid fibrils could be used as biomimetic scaffold material for cartilage tissue regeneration. A previous work supports this hypothesis since amyloid fibrils support cell attachment[23] and can undergo relaxation upon the application of force,[24] both important cues for cell behavior.[25] In addition, micrometer-sized gel particles of amyloid fibrils, so-called amyloid micronetworks (AMN), can be generated using a lab-on-a-chip approach[26] or by controlling self-assembly conditions.[27] Combining AMN with cells would allow minimal invasive application of the AMN and cells in a defect.

Recent studies show promising results for amyloid-based scaffolds of β-lactoglobulin (βLG),[28] lysozyme (LZ),[29] and amyloid-β.[30,31] The protein used for self-assembly influences

Received: January 9, 2023
Accepted: May 18, 2023

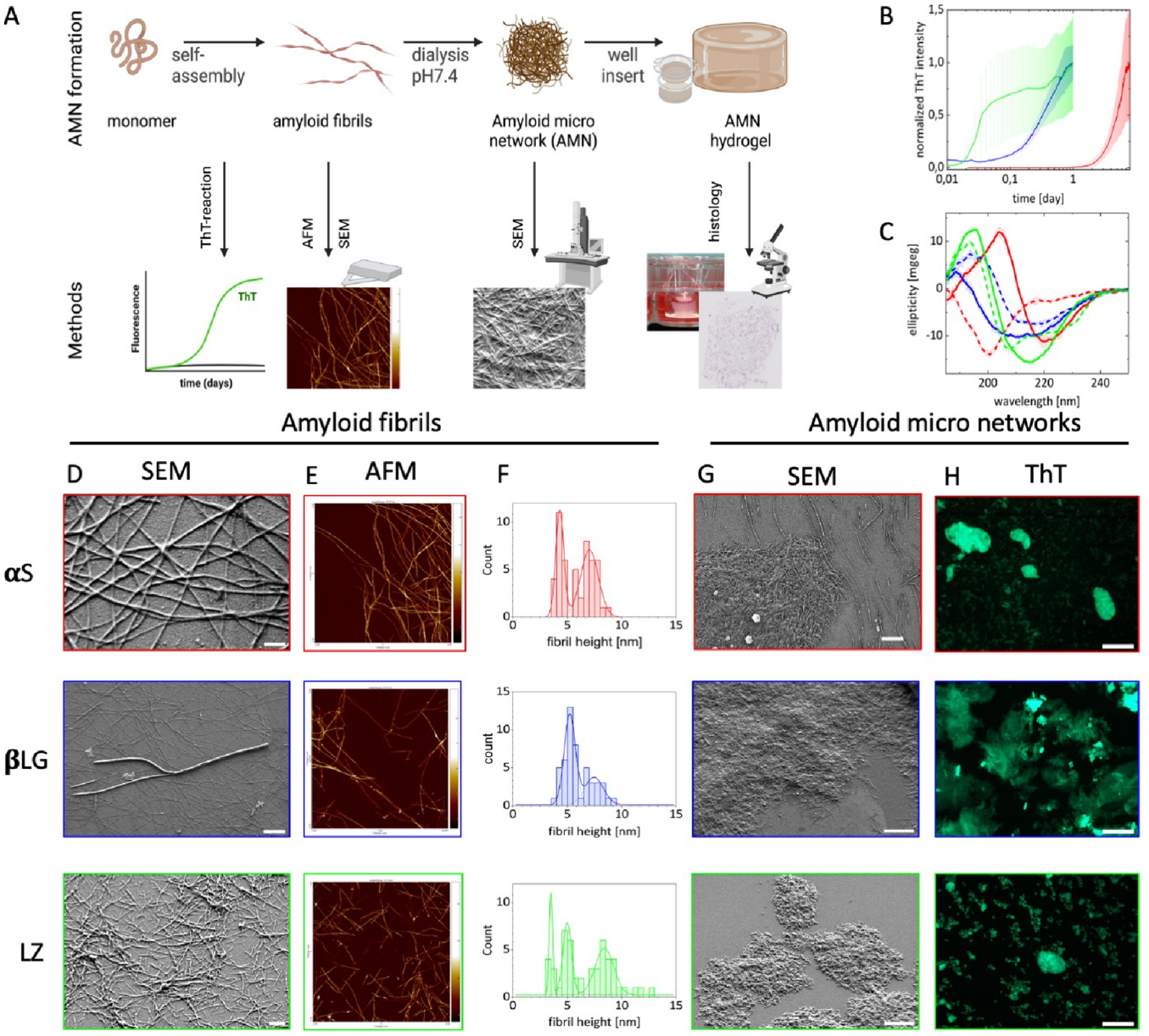

Figure 1. Self-assembly of amyloid fibrils and verification of amyloid micronetwork formation. (A) AMN formation and methods used to assess fibrils and amyloid micronetworks; figure generated in BioRender. (B) Fluorescence signal increase, due to binding of ThT to amyloid fibrils during self-assembly for αS (red), βLG (blue), and LZ (green), suggest that amyloid structures are formed. The ThT fluorescence reached a plateau after 165 h (86% of incubation time) for αS, 20 h (83%) for βLG, and 5 and 16 h (21 and 65%) for LZ. (C) CD-spectroscopy results for αS (red), βLG (blue), and LZ (green) before (open line) and after (closed line) incubation showing an increase in β-sheet content after incubation. (D) SEM images of αS (scale bare 200 nm), βLG (scale bare 1 μm), and LZ (scale bare 400 nm) revealing fibrils with various morphologies. (E) AFM images of 5 × 5 μm surfaces with αS (scale bare −2 - 18 nm), βLG (scale bare −2 − 25 nm), and LZ (scale bare −2 - 36 nm) fibrils. (F) Height distribution from AFM images of αS fibrils (peaks at 4 and 7 nm), βLG fibrils (peaks at 5 and 7 nm), and LZ fibrils (peaks at 3, 5, and 8 nm) showing the presence of various subpopulations of fibrils. (G) SEM revealing fibrous AMN of tens of micrometers in diameter for fibrils of αS, βLG, and LZ. Scale bar 2 μm. (H) The AMN of αS, βLG, and LZ retained their ability to bind ThT and thus remained amyloid-like. Scale bar 100 μm.

the properties of the brush-like structure of amyloid fibrils.[32] Depending on the amino acid sequence of the protein, the properties of the peptide sequence protruding from the fibril core differs. By producing amyloid fibrils of different proteins, it is possible to influence the cell's local environment, thereby influencing the cells' behavior. We therefore hypothesized that the protein used to form the AMN influences the formation of ECM.

To test this hypothesis for cartilage tissue regeneration, we selected βLG, LZ, and αS as amyloid forming proteins. LZ is native to the joint,[33] αS to the body, and βLG is non-native. βLG[28] and LZ[29] have been successfully studied as scaffold material. We included alpha-synuclein (αS) as the third protein. This protein is linked to Parkinson's disease and a subject of many studies in our lab.[14,34,35] All three proteins are known to form amyloid fold fibrils. αS and LZ are incorporated as full protein in amyloid fibrils, while βLG fibrils consist of

https://doi.org/10.1021/acsomega.3c00151
ACS Omega XXXX, XXX, XXX−XXX

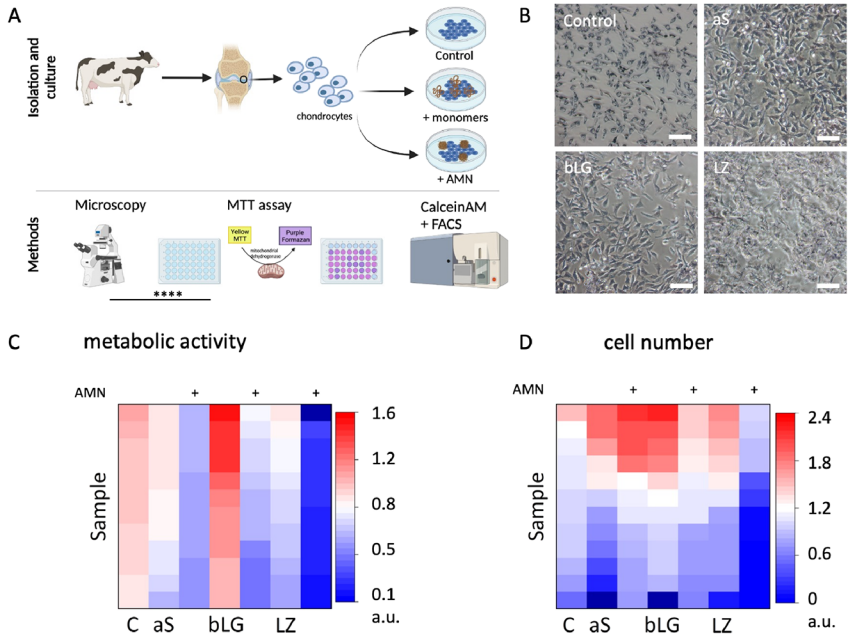

Figure 2. Chondrocyte viability after culture with AMN. (A) Chondrocyte isolation and culture conditions and methods of analysis; figure generated in BioRender. (B) Representative images of chondrocytes (blue due to formazan crystals) during culture with α-synuclein (aS), β-lactoglobulin (bLG), or lysozyme (LZ) (AMN appear as transparent structures). Scale bar 100 μm. (C) Heatmap of the total metabolic activity (MTT) in the presence of protein monomers and AMNs. The metabolic activity is reduced when chondrocytes are cultured in the presence of AMN (indicated by +) βLG monomers increase metabolic activity as compared with control. (D) Heatmap of the relative cell numbers in the presence of protein monomers and AMNs. The chondrocyte cell number did not change significantly between conditions during culture.

peptide fragments that form upon hydrolysis.[36] The physicochemical properties resulting from the amino acid sequences differs between the proteins. The proteins differ in their net charge, while they have comparable MWs: 14.3 kDa for αS, 18.4 kDa for βLG, and 14.6 kDa for LZ.

We investigated the short-term effects of AMN on chondrocyte viability and evaluated ECM formation after prolonged culture. To our knowledge, this is the first study providing a side-by-side comparison of the effect of the protein used to form amyloid structures on cartilage ECM formation.

RESULTS

α-Synuclein, β-Lactoglobulin, and Lysozyme Self-Assembled into Amyloid Fibrils. Before assessing the potential use of amyloid structures for cartilage tissue engineering, we verified that our protocols resulted in amyloid fibrils for the proteins α-synuclein (αS), β-lactoglobulin (βLG), and lysozyme (LZ) (Figure 1A). The solutions containing the different proteins became Thioflavin T (ThT) positive during incubation (Figure 1B). The increase in ThT intensity with time shows that the proteins assemble into amyloid structures. All ThT signals reached a plateau during incubation as fibril self-assembly slowed down with the consumption of protein monomers until equilibrium was reached. The amount of protein that self-assembled into amyloid structures was determined by measuring the protein in the supernatant after centrifugation using UV−vis spectroscopy. αS had a yield of ∼65% and LZ of >95%. The yield of BLG self-assembly could not be determined in a similar fashion, as BLG is known to hydrolyze in one or more peptides under self-assembly conditions,[36] and was therefore assumed to be comparable to LZ for further experiments. The secondary structure after self-assembly was investigated to confirm the amyloid nature. Circular dichroism spectra revealed a change from the protein's native secondary structure to one rich in β-sheets and unstructured domains (Figure 1C). These results indicate that the used protocols result in amyloid-like assemblies.

The formation of fibrils during incubation was confirmed using SEM (Figure 1D). Images revealed fibrils of αS and βLG of at least a micrometer in length (Figure 1D), while LZ fibril length varied between 0.2 μm and several micrometers (Figure 1D). AFM images confirmed the formation of fibrils, and the diameter of the fibrils was determined from AFM images (Figure 1E,F). Thicker or intertwined fibrils were observed for all three proteins, visible as subpopulations in the AFM height histograms. Intertwining amyloid fibrils and variations in fibril morphology are known in literature,[37,38] but their effect is beyond the scope of this work since these parameters not only depend on amino acid sequence but also on incubation conditions. Based on these results, we conclude that our protocols resulted in self-assembly of amyloid fibrils from αS, βLG, and LZ. The solutions containing the amyloid fibrils were collected for self-assembly into AMN.

Fibrils of all Three Proteins Formed Amyloid Micronetworks. Introducing salts to, or changing the pH of, a solution of amyloid fibrils, can induce self-assembly of amyloid fibrils into micrometer-scale amyloid micronetworks (AMN).[27] We dialyzed the obtained amyloid fibril solutions against PBS to induce the formation of such AMN and imaged samples from the resulting solutions (Figure 1A). SEM images of dried samples revealed fibrous AMN of tens of micrometers in diameter (Figure 1G). Fluorescence microscopy demonstrated that the AMN remained ThT positive after self-assembly and thus consisted of amyloid fibrils (Figure 1H). The AMN in solution vary in size and occasionally span more than 100 μm. αS AMN were comparable to previously described AMN,[27] and LZ AMN have similar morphologies to αS AMN. βLG

https://doi.org/10.1021/acsomega.3c00151
ACS Omega XXXX, XXX, XXX−XXX

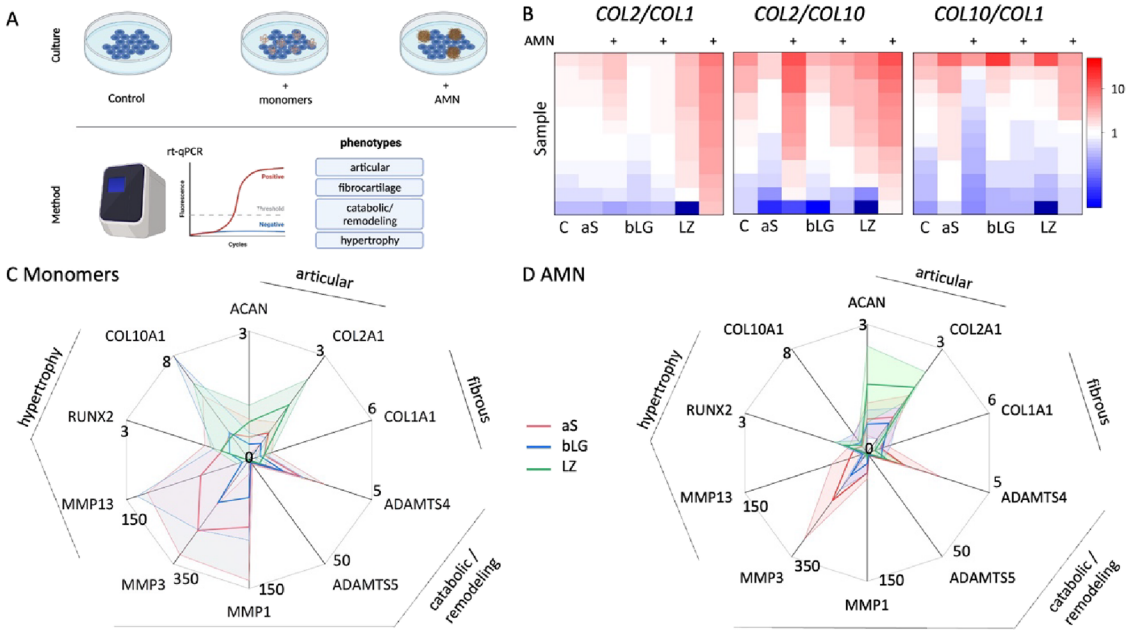

Figure 3. Comparison of gene expression levels after 3 days of culture. (A) Experimental setup to measure relative mRNA levels of cartilage related genes in chondrocytes after 3 days in culture with no protein monomers or AMNs (control, used for normalization), or protein monomers and AMNs of α-synuclein (aS, red), β-lactoglobulin (bLG, blue), or lysozyme (LZ, green). Figure generated in BioRender. (B) Heatmaps of the ratio of *COL2A1/COL1A1, COL2A1/Col10A1*, and *Col10A1/Col1A1* to compare phenotype specific collagen expression showing that the presence of LZ results in an articular cartilage phenotype as there is an increase in collagen 2 expression as compared to collagen 1 and 10. AMN are indicated by "+". (C) Spider plot of qPCR data of cells cultured with monomers of α-synuclein (αS, red), β-lactoglobulin (βLG, blue), or lysozyme (LZ, green) normalized to a control to which no protein is added. *Y*-Axes indicate fold change in expression in comparison to the control. Genes are grouped per phenotype. (D) Spider plot of qPCR data of cells cultured with amyloid micronetworks (AMN) of α-synuclein (αS, red), β-lactoglobulin (βLG, blue), or lysozyme (LZ, green), normalized to a control to which no protein is added. *Y*-Axes indicate fold change in expression in comparison to the control. Genes are grouped per phenotype.

AMN appear sheet-like and have larger diameters in comparison to αS and LZ AMN. Thus, dialysis of αS, βLG, and LZ amyloid fibrils resulted in AMN assembly. The AMN were dialyzed against cell culture medium (DMEM) in preparation of cell culture experiments.

Chondrocyte Viability Is Maintained in the Presence of Amyloid Micronetworks. We investigated the overall effect of our AMN on chondrocyte viability (Figure 2A). Bovine chondrocytes were cultured for 3 days as a monolayer in the absence (control) or presence of the different AMN. In the presence of different AMN, the chondrocytes were able to attach and grow and retained a normal morphology (Figure 2B). The total metabolic activity per sample was determined with MTT assays as a measure of cell viability (Figure 2C). This experiment was performed for both equivalent monomer concentrations of monomeric proteins and AMN to determine whether changes in metabolic activity are caused by the amyloid structures or by the increased protein concentration. The metabolic activity is presented as a heatmap of each individual sample for both monomers (left column for each protein) and AMN (right column for each protein, Figure 2C). The presence of AMN decreased the total metabolic activity as compared to the control with ~40% due to αS ($p = 0.002$) and βLG ($p = 0.003$) AMN. Both LZ monomers and LZ AMN reduced the metabolic activity by ~80% as compared to the control ($p < 0.001$). LZ AMN reduced metabolic activity by ~40% as compared to αS ($p = 0.004$) or βLG ($p = 0.002$) AMN (Figure 2C). βLG monomers increased the total activity with ~50% in relation to αS ($p = 0.027$) and LZ ($p = 0.007$) monomers (Figure 2C). The metabolic activity in the presence of monomers was not decreased to a similar extent as in the presence of AMN. This indicates that the decreased total metabolic activity can be attributed to the presence of AMN and not to the increased protein concentration.

The reduction of total metabolic activity may be attributed to previously reported cytotoxic effect of αS,[39] βLG,[40] and LZ[41,42] amyloid fibrils. However, the cells were regularly inspected with light microscopy and no apparent differences between conditions were observed (Figure 2B). We suspected that the decrease in metabolic activity was not indicative for cell viability and continued to investigate the cellular response to AMN. Assuming control chondrocytes continued to proliferate and dedifferentiate as described before,[43,44] changes in total metabolic activity can be explained by various causes: (1) AMN are cytotoxic and cell numbers reduce in their presence; (2) AMN prevent proliferation, and cell numbers only increase in the control condition; and (3) AMN alter the phenotype of the cells, resulting in differences in gene expression levels and thus in differences in activated metabolic pathways.

To investigate the underlying cause of the decrease in total metabolic in the presence of AMN, we cultured chondrocytes as described before, stained them with calcein-AM, and quantified them with flow cytometry, a different method to probe cell viability. Healthy cells will take up the dye, which becomes fluorescent by enzymatic cleavage of the AM part, while cells with compromised membranes have a reduced fluorescence signal due to leakage of the dye that can be distinguished from healthy cells' fluorescence signal. The percentage chondrocytes with intact membranes was ~90%

https://doi.org/10.1021/acsomega.3c00151
ACS Omega XXXX, XXX, XXX−XXX

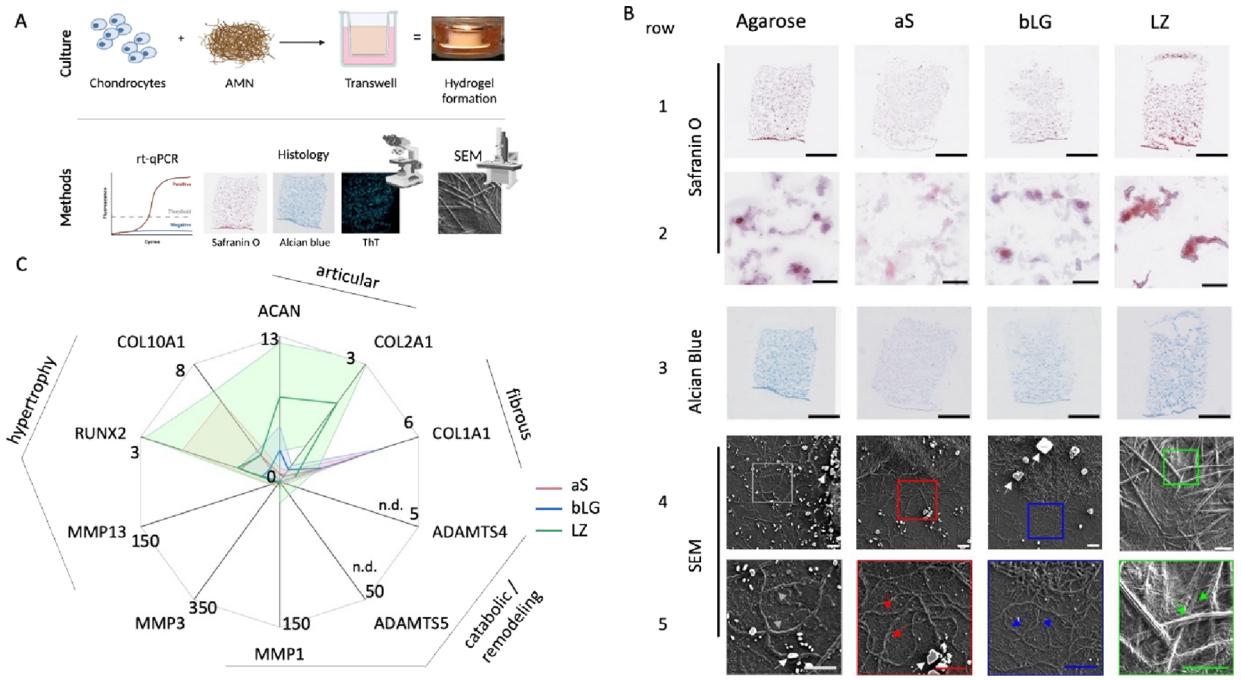

Figure 4. Comparison of gene expression levels and extracellular matrix deposition after 5 weeks of culture. (A) Chondrocytes were cultured for 5 weeks in hydrogels of agarose (control, gray) or in amyloid micronetworks (AMN) of α-synuclein (αS, red), β-lactoglobulin (βLG, blue), or lysozyme (LZ, green); figure generated in BioRender. (B) Representative images of vertical cross sections of agarose or AMN mixed with chondrocytes after 5 weeks of culture. Row 1: sections stained with safranin O (glycosaminoglycans) and hematoxylin (nuclei; scale bar 2 mm). Row 2: close-ups of sections stained with safranin O (glycosaminoglycans) and hematoxylin (nuclei; scale bars represent 100 μm). Row 3: sections stained with Alcian blue (scale bar 2 mm). The membrane of the well insert can be observed at the bottom of the images. Row 4: representative SEM images of sections after 5 weeks of 3D culture. Agarose (scale bar 2 μm), αS AMN (scale bar 1 μm), βLG AMN (scale bar 1 μm), and LZ (scale bar 3 μm). Row 5: close-up of images in row 4, as indicated by colored squares. Intertwined bundles can be observed in agarose (gray arrows, scale bar 2 μm), αS (red arrow, scale bar 1 μm), and βLG AMN (blue arrows, scale bar 1 μm). In contrast, collagen bundles with typical D-banding (green arrows) are observed in the LZ AMN section (scale bar 3 μm). Multiple images contain crystalline white particles, which are possibly salt crystals formed during drying of the sections (white arrows). (C) Spider plot of gene expression after 5 weeks in hydrogels of αS (red), bLG (blue), and LZ (green), normalized to agarose control. *Y*-Axes indicate fold change in expression in comparison to the control. Please note that the scale for ACAN is increased to 13 in the 5 week culture to allow visualizing the increase in ACAN expression at this time-point. Genes grouped per phenotype.

and did not vary between the conditions for either monomers (Figure S1A) or AMN (Figure S1D). Flow cytometry also measures cell size (forward scatter) and granularity (side scatter), and both increase and reduction of either parameter are related to decreased viability.[45,46] Neither parameter was affected by the presence of monomers or AMN (Figure S1B–F). Flow cytometry was also used to determine the number of cells present per volume as indicator of the total cell number after 3 days of culture. Although the inter-sample variation is high, both monomers and AMN (Figure 2D) did not significantly alter cell numbers between conditions.

We therefore conclude that the overall viability of the chondrocytes was not compromised, but metabolic activity detected with MTT assays was lowered due to the presence of AMN. These results also indicate that the total metabolic activity per samples was not affected by changes in the cell number and therefore exclude possible causes (1) (AMN are cytotoxic, and cell numbers reduce in their presence) and (2) (AMN prevent proliferation, and cell numbers only increase in the control condition).

Lysozyme Amyloid Micronetworks Support an Articular Cartilage Phenotype. The changes in the metabolic rate of the cultured chondrocytes might indicate changes in gene expression levels and thus the phenotype. Chondrocytes are known to quickly lose their phenotype during culture,[43] as early as the first passage.[44] The observed decrease in metabolic activity could therefore be indicative of the maintained phenotype of the chondrocytes in our assays. We therefore quantified mRNA levels with qPCR to test the effect of monomeric proteins and AMN of αS, βLG, or LZ on genes indicative of an articular, fibrocartilage, matrix remodeling, or hypertrophic phenotype after 3 days of monolayer culture (Figure 3A).

Correct ECM formation is required for tissue formation and regeneration. Different cartilage phenotypes can be distinguished by quantifying expression of different types of genes. Expression of the genes *ACAN* (aggrecan in proteoglycans) and *COL2A1* (type 2 collagen) is specific for articular cartilage, while *COL1A1* (type 1 collagen) is specifically found in in fibrous cartilage. In cartilage development and homeostasis, remodeling and repair occurs by degradation of collagen by collagenases MMP1 and MMP3 and aggrecan by aggrecanases ADAMTS4 and ADAMTS5. Excessive expression of their genes, however, leads to tissue degradation as observed in osteoarthritis.[47] Chondrocytes become hypertrophic during normal development of the growth plate but also during disease, resulting in endochondral ossification characterized by expression of RUNX2, COL10A1, and MMP13.[47−49]

An indication for the phenotype can be obtained by taking the ratio of expression of the different collagens, with collagen

https://doi.org/10.1021/acsomega.3c00151
ACS Omega XXXX, XXX, XXX−XXX

1 being indicative of fibrous, collagen 2 of articular, and collagen 10 of hypertrophic cartilage. Both LZ and αS AMN, but not the monomers, favor an articular cartilage phenotype over fibrous (*COL2A1*/*COL1A1*) or hypertrophic (*COL2A1*/*COL10A1*) phenotype, whereas there is a small increase in hypertrophic over fibrous (*COL10A1*/*COL1A1*) cartilage for the monomers (Figure 3B), indicating that both LZ and αS monomers slightly favor a hypertrophic (endochondral) phenotype. For LZ, both monomers and AMN show an increased articular cartilage phenotype when comparing the ratios *COL2A1*/*COL1A1* (∼4-fold, $p < 0.001$) and *COL2A1*/*COL10A1* (∼5-fold, $p = 0.005$), indicating that LZ supports an articular cartilage phenotype.

The data show that cells cultured in the presence of either LZ monomers (Figure 3C) or AMN (Figure 3D) preferentially increased gene expression of articular cartilage genes *ACAN* and *COL2A1*, whereas αS seems to support expression of genes associated with remodeling or a catabolic phenotype, especially for the monomers. Expression of *ACAN*, *COL2A1*, or *COL1A1* was not affected by βLG AMN (Figure S2), indicating that these AMN do not enhance articular cartilage formation, as illustrated with the ratio of *COL2A1* over *COL1A1* (Figure 3D).

Cells cultured in the presence of αS or βLG preferentially expressed genes associated with matrix remodeling and catabolism (Figure 3C,D). αS AMN increased the expression of *MMP1* in relation to the control and to LZ AMN (Figure S2). αS monomers significantly increased *MMP3* expression as compared to the control and to LZ monomers (Figure S2). LZ AMN decreased *ADAMTS5* expression in relation to the control, αS AMN, and βLG AMN (Figure S2).

The presence of βLG seemed to slightly increase gene expression associated with cartilage hypertrophy MMP13 and COL10A1, as compared to the other proteins, but this is due to the high standard deviation, as no significant changes in expression were observed. *RUNX2* expression was lowered by the presence of all amyloid proteins (Figure S2), indicating that AMN or the various proteins do not induce hypertrophy in chondrocytes within 3 days.

Interestingly, addition of monomers of the various proteins resulted in similar expression levels as did addition of AMN, where LZ supported the formation of articular cartilage, indicating that the amyloid structure was not required to induce these changes in gene expression.

Taken together, these results show that AMN affect both the metabolic activity and gene expression levels within 3 days. LZ AMN appear to support articular cartilage tissue formation and to decrease total metabolic activity of the chondrocytes. αS and βLG AMN seem to induce collagen breakdown, which would result in either tissue remodeling or degradation. This also suggests that the observed decrease in metabolic activity is caused by (3) AMN altering the chondrocytes' phenotype, resulting in differences in gene expression levels. We therefore expect that AMN could support cartilage tissue regeneration, but tissue formation might depend on which protein is used to make the AMN.

Lysozyme Amyloid Micronetworks Stimulate Extracellular Matrix Deposition. For AMN to be successful, long-term exposure of chondrocytes to AMN should maintain the chondrocytes' phenotype and support tissue formation. We cultured chondrocytes mixed with AMN in culture inserts to investigate ECM deposition and cartilage marker gene expression after 3D culture for 5 weeks (Figure 4A, Figure S3A).

To investigate ECM deposition, we stained vertical sections of the contents of the inserts with safranin O and Alcian blue to investigate glycosaminoglycans deposition. In addition, vertical sections were imaged to investigate collagen deposition using SEM (Figure 4B).

Glycosaminoglycan production was observed as reddish areas in the sections (Figure 4B, top panel). A closer examination revealed that glycosaminoglycan deposition is limited to patches throughout the section around chondrocytes (counterstained with hematoxylin, Figure 4B, second row). Sections of αS and βLG AMN samples contained glycosaminoglycans in a lower amount as compared to the agarose control. LZ AMN increased the number and intensity of glycosaminoglycan depositions throughout the section in comparison to the other conditions, indicating an increased amount of glycosaminoglycans. These results were confirmed with the Alcian blue staining (Figure 4B, third row). Together, these findings indicate that glycosaminoglycans were deposited in increased amounts in the presence of LZ AMN but not in the presence of αS and βLG AMN as compared to agarose or LZ AMN.

We investigated whether AMN were replaced by or coexisted with newly formed ECM after 5 weeks of culture. Sections were stained with ThT to confirm that the amyloid nature was preserved during culture. All AMN remained ThT positive, while agarose stained negative (Figure 3B).

SEM was used to investigate if collagen fibers, the other main component of cartilage ECM, were present (Figure 4B, rows 4 and 5). Collagen can be recognized because the fibers are often straight and have a larger diameter ∼1−10 μm) than amyloid fibrils (5−10 nm, Figure 1F). In addition, collagen fibers can be recognized by the so-called D-banding. Few to no straight bundles were observed in agarose, αS AMN, and βLG AMN sections (Figure 4B, rows 4 and 5). LZ AMN sections contained straight bundles with larger diameters than amyloid fibrils. The close-up revealed the D-band characteristic of collagen bundles, confirming the deposition of collagen bundles (indicated by green arrows). Sections of agarose, αS AMN, and βLG AMN samples contained bundles, but these lacked the characteristic D-banding of collagen. These other bundles appear thicker and longer than the amyloid fibrils in AMN but intertwined instead of being regularly packed as expected of collagen bundles (indicated by gray, red, and blue arrows). Thus, all sections contained deposited bundles, but only LZ AMN supported the formation of packed bundles with D-banding as expected of collagen bundles.

The observations from histological and SEM images confirmed that LZ AMN support glycosaminoglycan and collagen deposition, while αS AMN and βLG AMN result in limited ECM formation. The protein used to form AMN thus determines whether AMN support tissue regeneration.

Lysozyme Amyloid Micronetworks Sustained the Articular Cartilage Phenotype after Five Weeks of Culture. Articular cartilage tissue formation is expected when *ACAN* and *COL2A1* are upregulated, while *COL1A1* (fibrous cartilage marker) and COL10A1 (hypertrophic/endochondral cartilage marker) are downregulated. A spider plot of the qPCR data shows an increase of articular cartilage markers in cells grown in LZ, but not in the other AMN (Figure 4C). In some samples of LZ, we also observed an increase in expression of the hypertrophic marker RUNX2,

https://doi.org/10.1021/acsomega.3c00151
ACS Omega XXXX, XXX, XXX−XXX

suggesting a transition to a hypertrophic phenotype. However, this did not lead to an increase in *COL10A1* expression. Expression of *RUNX2*, *COL10A1*, and *MMP13* was not significantly influenced by the various AMN. The various AMN did not affect expression of COL1A1.

At this time-point, we could not detect ADAMTS4/5 and the expression of MMPs was much lower than that measured after 3 days in culture (Figures S2 and S4). Expression of *MMP1* and *MMP3* was increased by the proteins αS and βLG after 3 days, but this trend changed after 5 weeks, when MMP expression was no longer detected at the same scale. Cells cultured in αS AMN show some markers of hypertrophy (*RUNX2*, *COL10A1*), but no significant differences are found as compared to the control or other AMN.

Together, our data shows that LZ AMN sustained the chondrocytes' phenotype for 5 weeks and favor articular cartilage formation during culture.

DISCUSSION

Restoring damaged articular cartilage to its native state remains a scientific and clinical challenge. Here, we investigated the potential of amyloid-based scaffolds for cartilage tissue regeneration. For this, we produced AMN via self-assembly from the proteins αS, βLG, or LZ and cultured chondrocytes in the presence these AMN to study their effect on cartilage ECM formation.

Our results show that successful articular cartilage tissue formation can be supported by AMN, but only LZ AMN resulted in tissue formation. The cross-β sheet amyloid structure is present in the AMN of all proteins used and can therefore not be the determining factor. The difference in effectiveness of AMN to induce tissue regeneration correlates with the calculated net charge of the proteins at neutral pH (PROTEIN CALCULATOR v3.4): αS monomers have a net charge of −9e, and peptides resulting from βLG hydrolysis[36] have net charges between −5e and 1e, while LZ has a net charge of +7e. The effect of net charge of the scaffolds on tissue regeneration has been reported before. Various cell types respond to surfaces with different charge valence[50] or net charge,[51−53] and this results in differences in attachment,[50,51,53] morphology,[50−52] proliferation,[50−52] cellular processes,[51−53] and protein absorption to the surface.[50−52] However, the sign of the net charge is not the sole predictive for the mentioned effects. Whether the net charge itself or the resulting adsorption with matrix proteins and other components, as we observed for binding of serum albumin to lysozyme fibrils,[22] is responsible for the observed trend remains to be investigated.

Using AMN for a scaffold provides control over the net charge by choosing the protein to self-assemble into AMN. However, cells also respond for instance to the nanoscale topography[54] and mechanical properties.[31] Our protocol resulted in AMN with various fibril diameters and morphologies, which could influence the chondrocytes' response and the effectiveness of the used AMN to support ECM deposition.

It has been shown that scaffold topographies[55−57] and matrix mechanical properties including elasticity and stiffness[58−60] play an important role in (cartilage) tissue formation and maintenance. As such, the rheological properties of the hydrogel used for tissue regeneration are key in determining cell fate. It has been described that attractive interfibril interactions are responsible for the viscoelastic response of amyloid networks as a function of frequency, as shown for amyloid networks composed of α-synuclein,[14] β-lactoglobulin,[61] and lysozyme.[22] Here, we have not focused on the material properties but instead have observed that the choice of protein determined the gene expression of the cultured chondrocytes rather than the structure of the corresponding amyloid micronetworks.

All used proteins supported cartilage formation to a certain extent, as glycosaminoglycan production and gene expression characteristic of cartilage were detected. However, only cells cultured for prolonged time in a 3D hydrogel composed of LZ AMN were able to correctly produce collagen bundles. Correctly formed collagen bundles show a characteristic D-banding and provide tensile strength to the tissue to resist deformation. Chondrocytes cultured in the presence of all AMN produced intertwined bundles that were structurally different from straight collagen bundles and amyloid. These bundles lack D-banding and may consist of collagen molecules that could not successfully assemble. The diameter of the flexible intermediate structures observed during the assembly of D-banded collagen fibrils is smaller than or comparable to amyloid fibrils,[62,63] while the diameter of the intertwined bundles is comparable to or larger than the diameter of amyloid fibrils. This indicates that assembly of collagen bundles, but not of the smaller collagen fibrils, is hindered. The absence of correctly assembled collagen bundles coincided with increased relative mRNA expression levels of *MMP1*, *MMP3*, and *MMP13* after 3 days. The literature suggests that degeneration of collagen bundles by MMP1 results in structures that are more bended, while the presence of MMP13 results in split bundles.[64] The increased expression of *MMP1* and *MMP13* in our experiments thus give a possible explanation for the strange appearance of the bundles in our samples.

Proteoglycans, the other required main cartilage ECM component, consist of highly negatively charged glycosaminoglycan molecules linked to aggrecan that attract counter ions. The resulting osmotic pressure resists compression. In healthy ECM, proteoglycans form an interconnected network with collagen. Proteoglycans containing decorin[65] and aggrecan[66] were reported to stabilize collagen bundles and protect the bundles from degradation by MMPs. Chondrocytes cultured with LZ AMN increased glycosaminoglycan deposition and resulted in an upregulation of *ACAN* mRNA levels, both indicative of increased proteoglycan deposition. In αS or βLG AMN, we could not observe D-banded collagen type 2 bundles. Proper tissue formation thus seems to be hampered by a lack of proteoglycans to protect and stabilize collagen bundles, and this varies with the AMN used in culture.

We monitored chondrocyte viability during culture in the presence of AMN and found seemingly conflicting results after 3 days. The overall viability of the chondrocytes remained constant and light microscopy images did not reveal changes in the chondrocyte phenotype. However, chondrocyte metabolism was affected: the presence of AMN reduced oxidoreductase activity (MTT) of the chondrocytes, while their esterase activity (calcein-AM) remained unaffected. These results were not indicative of tissue formation after 5 weeks: only LZ AMN produced ECM constituents. qPCR results were indicative of ECM deposition after 5 weeks (Figures 6 and 7). As the number of cells remained constant between conditions, the difference in oxidoreductase activity cannot be explained by the cell number. However, chondrocytes have a relatively

https://doi.org/10.1021/acsomega.3c00151
ACS Omega XXXX, XXX, XXX−XXX

low number of mitochondria,[67] and decreased activity might therefore be an indicator of the chondrocyte dedifferentiation. Dedifferentiation would also explain the relatively low *ACAN* and *COL2A1* expression levels and ECM deposition in the control and αS AMN and βLG AMN conditions. As (de)differentiation of cells changes their metabolic activity[68] and gene expression profile,[43,44] it is not unlikely that changes arise as a result of the cellular response to the different AMN. Yet, this makes determining the viability of cells complex, as most assays measure the amount present of a single enzyme. A better defined metabolic and gene expression make-up of chondrocytes suitable for tissue regeneration would be beneficial to determine which markers to monitor and to determine how chondrocytes respond to regeneration strategies.

In this study, we investigated αS-, βLG-, and LZ-based AMN as model systems for amyloid-based scaffolds due to their previous implications as scaffold material and comparable amyloid structure yet different features, such as net charge. We demonstrate differences in cellular response upon exposure to the various proteins, indicating that the protein properties influence the cell's response and not the protein amyloid network per se. Future tissue engineering strategies for cartilage repair are aimed for instructive scaffolds that provide a mechanically stable environment, are preferably cell-free and allow for cell migration into the scaffold, and maintain cell viability and promote cartilage-specific matrix production in vitro.[7,69,70] Our labs have extensive experience in generation of synthetic injectable hydrogels for cartilage repair[7,69,71−73] that are now in clinical trials.[74] While LZ, βLG, and αS may not be directly used as amyloid fold networks for tissue regeneration due to their role in bacteriolysis and/or systemic amyloidosis[33,36] and Parkinson's disease,[75] exploratory studies such as ours aid in isolating the relevant properties for the design of a scaffold and can assist with selecting suitable proteins in future studies.

■ CONCLUSIONS

All results combined confirm that AMN can be used as scaffold material for cartilage tissue engineering. Cell viability was not compromised, and all conditions contained evidence of ECM deposition. However, the cellular response to the different AMN varied and only LZ AMN supported the deposition of proteoglycans and collagen bundles required for articular cartilage tissue restoration. While amyloid structures are usable as scaffold materials, it is the protein used to self-assemble the AMN that determines if tissue regeneration will be successful.

■ MATERIALS AND METHODS

Self-Assembly of Amyloid Micronetworks. Protocols to form amyloid fibrils were adapted from literature for α-synuclein (αS),[76] β-lactoglobulin (βLG),[36,77] and chicken egg white lysozyme (LZ).[78,79] All chemicals are from Merck, and all solutions were prepared in ultrapure water, unless otherwise noted. In short, a solution of 1 mM recombinant αS in 10 mM tris(hydroxymethyl)aminomethane, pH 7.4 (Sigma-Aldrich), 10 mM NaCl, and 100 μM Na_2EDTA was incubated at 37 °C and 750 rpm for 8 days. A solution of 1 mM bovine βLG (Sigma-Aldrich), pH = 2 (with HCl), was incubated at 80 °C and 750 rpm for 1 day. A 1 mM chicken egg white LZ (Sigma-Aldrich) in 50 mM NaH_2PO_4 and HCl at pH 2 was incubated for 1 day at 60 °C and 750 rpm. All solutions were sterilized through a 0.2 μm filter (Boom B.V.) prior to incubation.

Amyloid fibrils self-assembled in amyloid micronetworks (AMN) during dialysis to neutral pH (based on[27]). Solutions with fibrils were dialyzed three times against phosphate-buffered saline at pH 7.4 (PBS, Gibco) in a 100 kDa molecular weight cut off cellulose ester dialysis membrane (Spectrum) and one time against high glucose Dulbecco's modified Eagle medium (DMEM, Gibco) when used for cell culture.

Characterization of Amyloid Fibrils and AMN. Self-assembly of amyloid fibrils was followed by measuring the fluorescence signal (excitation: 466 nm, emission: 485 nm) due to Thioflavin T (ThT, Sigma-Aldrich) binding to fibrils during incubation. ThT (9.0 μM) was added to the solution of αS, and the fluorescence signal was captured during incubation with an Infinite 200 PRO multimode plate reader (Tecan). ThT (2.3 μM) was added to the βLG solution and 3.4 μM to the LZ solution. Their self-assembly was visualized with a Cary Eclipse fluorescence spectrophotometer (Varian).

Self-assembly efficiency was determined by measuring the concentration of protein remaining in solution after incubation using a UV2401 spectrophotometer (Shimadzu). Absorption was measured before and after centrifuging the samples for 3 min at 20,000*g* using $\varepsilon_{276\ nm}$ 5,600 M^{-1}, αS, $\varepsilon_{280\ nm}$ 17,600 M^{-1}, βLG,[80] and $\varepsilon_{280\ nm}$ 37,750 M^{-1}, LZ.[80]

Atomic force microscopy (AFM) images were used to confirm the formation of fibrils and determine their height. A Multimode 8 AFM (Bruker) was used to image fibril samples on mica in tapping mode (air) with a NCS36/CR-AU tip B (1.75 N/m, 155 kHz, MicroMasch). Height images were collected at 1024 × 1024 pixels and 0.1 Hz and used to determine the height of individual fibrils (N = 50) with a Scanning Probe Image Processor (6.0.13 by Image Metrology).

Amyloid fibril and AMN morphology were studied using a scanning electron microscope (SEM, MERLIN HR-SEM (Zeiss)). Fibrils were diluted 1000 times in ultrapure water, AMN 50 times, after incubation and deposited on silicon wafer squares. Samples were dried under ambient conditions prior to imaging. Images were processed with Fiji (Image J 1.52p[81]).

The amyloid nature of the AMN was confirmed by visualizing the AMN with fluorescence microscopy. AMN were diluted 10 times in ultrapure water with 90 μM ThT. Images were captured with an E400 fluorescence microscope (Nikon) and processed with Fiji.

Chondrocyte Isolation and Culture. Bovine chondrocytes were isolated from the knee of 10- to 12-month-old calves obtained from the local abattoir. Cartilage pieces were collected from the condyles, minced, and kept overnight in digestion medium containing 150 U/mL type 2 collagenase (Worthington) in DMEM with 10% heat inactivated foetal bovine serum (FBS, Sigma-Aldrich), 100 U/mL penicillin, and 100 μg/mL streptomycin (Gibco). The cells were filtered through a 200 μm cell strainer, washed 3 times with PBS, and stored at −80 °C in proliferation medium with 20% FBS and 10% dimethyl sulfoxide (Sigma-Aldrich). Chondrocyte proliferation medium consisted of DMEM with 10% FBS, 100 U/mL penicillin and 100 μg/mL streptomycin, 20 μM ascorbic acid (Sigma-Aldrich), 40 ug/mL L-proline (Sigma-Aldrich), and 1% MEM nonessential amino acid solution (Sigma-Aldrich).

Cells were seeded at 2500 cells/cm^2 in culture flasks (Nunc) with chondrocyte proliferation medium and cultured in hypoxic conditions: 37 °C, 95% humidity, 5% CO_2, and

https://doi.org/10.1021/acsomega.3c00151
ACS Omega XXXX, XXX, XXX−XXX

Table 1. Overview of Used Primer Sequences; *RPL13A* Was Used as the Housekeeping Gene

gene	forward (5′ to 3′)	reverse (5′ to 3′)
RPL13A	ATGCCCATACGGAACGTCTA	CAAGCCTCCCACGTACCAAA
ACAN	GACCAGAAGCTGTGCGAGGA	GCCAGATCATCACCACACAG
COL2A1	ATCAACGGTGGCTTCCACT	TTCGTGCAGCCATCCTTCAG
COL1A1	GCGGCTACGACTTGAGCTTC	CACGGTCACGGACCACATTG
MMP1	CTTTGATGGACCTGGTGGAAAC	AAATGAGCGTCTCCTCCGATAC
MMP3	AAGGGACAAGGAAGACACCA	TCACAATTCTGTACGTGAGGTGA
ADAM4	CTCCATGACAACTCGAAGCA	CTAGGAGACAGTGCCCGAAG
ADAM5	GGGACCATATGCTCTCCTGA	GCCAAGCAGATGTCCAATT
RUNX2	TTTTCAGACCCCAGGCAGTT	TTGGAGAAGCGGCTCTCAGT
COL10A1	CATGCTGCCACAAACAGC	TGGATGGTGGGCCTTTTA
MMP13	ATTCTTCTGGCGGCTGCATCC	AGGCGGCATCAATACGGTTGG

2.5% O_2. At 80% confluency, cells were trypsinized with 0.25% trypsin−EDTA (Gibco). Cells were used at passage 1, and a new donor was used for each experiment.

Chondrocyte Viability. Chondrocytes were adhered overnight, before addition of proliferation medium with no addition (control), or an equivalent of 95 μM monomers or AMN of αS, βLG, or LZ. After 3 days of culture, the cells were evaluated with an MTT assay, light microscopy, and flow cytometry.

The metabolic activity of the chondrocytes was determined by the MTT assay. Phenol red-free Dulbecco's modified Eagle medium (Gibco) was supplemented with 0.5 mg/mL 3-(4,5-dimethylthiazol-2-yl)-2,5-diphenyltetrazolium bromide (MTT, Sigma Aldrich). After 4 h of incubation, the medium was removed, and the resulting formazan crystals were dissolved in dimethyl sulfoxide. The formazan solution was centrifuged to remove cellular debris, and the absorbance of the supernatant was determined at 540 nm and corrected for background at 690 nm in a Multiskan GO microplate spectrophotometer (ThermoFisher Scientific).

Cell morphology was evaluated after incubation with MTT. Images of the cells including the formazan crystals were taken using a phase contrast Eclipse TE300 microscope (Nikon) with a DS Camera Control Unit DS-L2 (Nikon). Images were processed with ImageJ.

Calcein-AM staining (Invitrogen) was used to investigate cell membrane integrity. The chondrocytes were collected by treating them with trypsin and stained following the manufacturer's protocol. The resulting fluorescence signal was detected directly after resuspending the cells using a FACSCalibur (BD Biosciences) flow cytometer. Samples were measured until 20,000 events were detected; 100,000 in the case of AMN were present during culture; and the first 10 s of each measurement was used to determine the relative number of cells per sample. Cells were separated from AMN and debris using gates in Flowing Software (version 2.5.1, Turku Bioimaging). Similarly, the percentage cells with a high calcein signal and lower calcein signal (comparable to staining with ethidium homodimer) were determined from the total cell population.

ECM Deposition. Proliferation medium (200 μL) with 1.5 mM monomer equivalent of αS, βLG, or LZ AMN mixed with 5×10^6 cells/mL was added to a hanging cell culture insert (Millicell PIHT12R48, Millipore) and cultured in 1 mL of chondrocyte proliferation medium per well. AMN and cells precipitated to the bottom of the well overnight. Half of the medium in the wells was refreshed every 2 to 3 days. After 5 weeks, medium was removed from the wells prior to further processing.

The presence of glycosaminoglycans was determined by histology. Inserts (membrane and AMN-cell construct) were stored in their plates in a −30 °C freezer for a maximum of 7 days, before embedding in CryoMatrix (Thermo Scientific). Sections of 10 μm were collected on microscopy slides and stored at −30 °C until staining. Sections were stained with safranin O, with an additional step of 15 min in 0.5 w/v% ThT and 0.1 M HCl after rinsing, or Alcian blue, dehydrated, and sealed according to standard protocols. Slides were stored at 4 °C and imaged in the Nanozoomer (Hamamatsu). Images were processed with NDP.view 2.7.52 (Hamamatsu).

The presence of collagen was visualized by collecting sections on silicon wafers and imaging with SEM. Images were processed with Fiji, and collagen structures were distinguished from amyloid fibrils by diameter and the presence of D-bands.

Changes in Gene Expression. Relative changes in gene expression were studied using the quantitative polymerase chain reaction (qPCR). Chondrocytes were cultured for either 3 days or 5 weeks. RNA was isolated using TRIzol (ThermoFisher Scientific), according to the manufacturer's protocol. For the culture inserts, the content was collected after culture, dissolved in twice the required amount of TRIzol, left overnight on ice, and further homogenized. cDNA was synthesized with the iScript kit (Bio-Rad), and qPCR was performed using a SensiMix SYBR & Fluorescein Kit (Bioline) with primers (Sigma Aldrich) designed with Primer-BLAST (NCBI,[82] Table 1). Samples were measured in duplicate and resulting average C_T values analyzed according to the $2^{\Delta\Delta C_T}$ method to determine the fold change in expression in comparison to the control.[83]

Data Processing and Statistics. Data from amyloid characterization experiments was processed in Excel and visualized in Origin (OriginPro 2019b (64-bit) 9.6.5.169 (Academic) OriginLab Corporation). Data is depicted as the mean and standard deviation of four independent samples. Representative AFM and SEM image of amyloid fibrils and AMN were selected out of multiple batches, and the AFM images depicted were used to determine the height distribution.

Cell experiments were performed in triplicate with a unique donor and batch AMN per experiment and four samples per condition. Results are depicted in heatmaps, while qPCR results are displayed in spider plots. Images presented are representative for the three batches.

https://doi.org/10.1021/acsomega.3c00151
ACS Omega XXXX, XXX, XXX−XXX

Statistical analysis was performed with SPSS (IBM SPSS Statistics Version 25). Control sample values were rescaled to an average of one, and experimental conditions accordingly, to correct for donor and batch variation prior to statistical analyses. The data was first investigated with an ANOVA analysis of the combined data and, if $p < 0.200$, was followed by Bonferroni post-hoc tests to determine p-values. p-Values are reported if $p < 0.200$ as measure of strength for support of the hypothesis.

■ ASSOCIATED CONTENT

Supporting Information

The Supporting Information is available free of charge at https://pubs.acs.org/doi/10.1021/acsomega.3c00151.

Chondrocyte viability in the presence of protein monomers and networks with MTT assay and flow cytometry; chondrocyte gene expression levels after incubation with protein monomers and AMN by qPCR; presence of chondrocytes in 3D cultures after 5 weeks; and lysozyme amyloid micronetworks sustained the articular cartilage phenotype after 5 weeks of culture (PDF)

■ AUTHOR INFORMATION

Corresponding Author

Janine N. Post − *Developmental BioEngineering, TechMed Centre, University of Twente, Enschede, Overijssel 7500 AE, The Netherlands;* orcid.org/0000-0002-6645-6583; Phone: +31-53-4894205; Email: j.n.post@utwente.nl

Authors

Maurice C.E. van Dalen − *Developmental BioEngineering, TechMed Centre, University of Twente, Enschede, Overijssel 7500 AE, The Netherlands; Nanobiophysics, Mesa+, University of Twente, Enschede 7500AE, The Netherlands;* Present Address: Current address: Scinus Cell Expansion Netherlands B.V., Bilthoven, The Netherlands M.v.D

Marcel Karperien − *Developmental BioEngineering, TechMed Centre, University of Twente, Enschede, Overijssel 7500 AE, The Netherlands;* orcid.org/0000-0003-0751-0604

Mireille M.A.E. Claessens − *Nanobiophysics, Mesa+, University of Twente, Enschede 7500AE, The Netherlands;* orcid.org/0000-0002-2206-4422

Complete contact information is available at: https://pubs.acs.org/10.1021/acsomega.3c00151

Author Contributions

M.v.D. performed experiments; M.v.D., J.P., and M.M.A.E.C. analyzed data and generated all figures. The manuscript was written through contributions of all authors. All authors have given approval to the final version of the manuscript.

Funding

This work was funded by a Twente Graduate School stipend to M.v.D. and a Dutch Arthritis Foundation grant to M.K. and J.P.

Notes

The authors declare no competing financial interest.

■ ACKNOWLEDGMENTS

We thank Mark Smithers for taking the SEM images, Dr. Jacqueline Plass for Primer Design, Dr. Nathalie Fekete for FCM optimization and Kirsten van Leijenhorst−Groener for the αS production. We thank Dr. Kannan Govindaraj for help with statistics.

■ ABBREVIATIONS

αS	alpha synuclein
LZ	lysozyme
βLG	beta-lactoglobulin
AMN	amyloid micronetwork
ECM	extracellular matrix

■ REFERENCES

(1) Armiento, A. R.; Alini, M.; Stoddart, M. J. Articular fibrocartilage - Why does hyaline cartilage fail to repair? *Adv. Drug Delivery Rev.* **2019**, *146*, 289−305.

(2) Huey, D. J.; Hu, J. C.; Athanasiou, K. A. Unlike bone, cartilage regeneration remains elusive. *Science* **2012**, *338*, 917−921.

(3) Campos, Y.; Almirall, A.; Fuentes, G.; Bloem, H. L.; Kaijzel, E. L.; Cruz, L. J. Tissue Engineering: An Alternative to Repair Cartilage. *Tissue Eng., Part B* **2019**, *25*, 357−373.

(4) DiBartola, A. C.; Everhart, J. S.; Magnussen, R. A.; Carey, J. L.; Brophy, R. H.; Schmitt, L. C.; Flanigan, D. C. Correlation between histological outcome and surgical cartilage repair technique in the knee: A meta-analysis. *Knee* **2016**, *23*, 344−349.

(5) Roberts, S.; McCall, I. W.; Darby, A. J.; Menage, J.; Evans, H.; Harrison, P. E.; Richardson, J. B. Autologous chondrocyte implantation for cartilage repair: monitoring its success by magnetic resonance imaging and histology. *Arthritis Res. Ther.* **2002**, *5*, R60−R73.

(6) Maia, F. R.; Carvalho, M. R.; Oliveira, J. M.; Reis, R. L. Tissue Engineering Strategies for Osteochondral Repair. In *Advances in Experimental Medicine and Biology*, 1059 ed.; Springer, 2018; pp. 353−371.

(7) Fu, Y.; Zoetebier, B.; Both, S.; Dijkstra, P. J.; Karperien, M. Engineering of Optimized Hydrogel Formulations for Cartilage Repair. *Polymers* **2021**, *13*, 1526.

(8) Knowles, T. P. J.; Buehler, M. J. Nanomechanics of functional and pathological amyloid materials. *Nat. Nanotechnol.* **2011**, *6*, 469−479.

(9) Reynolds, N. P. Amyloid-like peptide nanofibrils as scaffolds for tissue engineering: Progress and challenges (Review). *Biointerphases* **2019**, *14*, No. 040801.

(10) Chiti, F.; Dobson, C. M. Protein Misfolding, Functional Amyloid, and Human Disease. *Annu. Rev. Biochem.* **2006**, *75*, 333−366.

(11) Goldschmidt, L.; Teng, P. K.; Riek, R.; Eisenberg, D. Identifying the amylome, proteins capable of forming amyloid-like fibrils. *Proc. Natl. Acad. Sci. U. S. A.* **2010**, *107*, 3487−3492.

(12) Guijarro, J. I.; Sunde, M.; Jones, J. A.; Campbell, I. D.; Dobson, C. M. Amyloid fibril formation by an SH3 domain. *Proc. Natl. Acad. Sci. U. S. A.* **1998**, *95*, 4224−4228.

(13) Pearce, F. G.; Mackintosh, S. H.; Gerrard, J. A. Formation of Amyloid-like Fibrils by Ovalbumin and Related Proteins under Conditions Relevant to Food Processing. *J. Agric. Food Chem.* **2007**, *55*, 318−322.

(14) Semerdzhiev, S. A.; Lindhoud, S.; Stefanovic, A.; Subramaniam, V.; Van Der Schoot, P.; Claessens, M. M. A. E. Hydrophobic-Interaction-Induced Stiffening of α -Synuclein Fibril Networks. *Phys. Rev. Lett.* **2018**, *120*, 1−6.

(15) Mackay, J. P.; Matthews, J. M.; Winefield, R. D.; Mackay, L. G.; Haverkamp, R. G.; Templeton, M. D. The hydrophobin EAS is largely unstructured in solution and functions by forming amyloid-like structures. *Structure* **2001**, *9*, 83−91.

(16) Barlow, D. E.; Dickinson, G. H.; Orihuela, B.; Kulp, J. L.; Rittschof, D.; Wahl, K. J. Characterization of the Adhesive Plaque of the Barnacle Balanus amphitrite : Amyloid-Like Nanofibrils Are a Major Component. *Langmuir* **2010**, *26*, 6549−6556.

(17) Maji, S. K.; Perrin, M. H.; Sawaya, M. R.; Jessberger, S.; Vadodaria, K.; Rissman, R. A.; Singru, P. S.; Nilsson, K. P. R.; Simon,

R.; Schubert, D.; et al. Functional amyloids as natural storage of peptide hormones in pituitary secretory granules. *Science* **2009**, *325*, 328−332.
(18) Bachmann, B.; Spitz, S.; Schädl, B.; Teuschl, A. H.; Redl, H.; Nürnberger, S.; Ertl, P. Stiffness Matters: Fine-Tuned Hydrogel Elasticity Alters Chondrogenic Redifferentiation. *Front. Bioeng. Biotechnol.* **2020**, *8*, 373.
(19) Barreto-Henriksson, H.; Llorente, M.; Larsson, A.; Brisby, H.; Gold, J.; Schuster, E.; Ström, A. Determination of mechanical and rheological properties of a cell-loaded peptide gel during ECM production. *Int. J. Pharm.* **2019**, *563*, 437−444.
(20) Lv, X.; Sun, C.; Hu, B.; Chen, S.; Wang, Z.; Wu, Q.; Fu, K.; Xia, Z.; Shao, Z.; Wang, B. Simultaneous Recruitment of Stem Cells and Chondrocytes Induced by a Functionalized Self-Assembling Peptide Hydrogel Improves Endogenous Cartilage Regeneration. *Front. Cell Develop. Biol.* **2020**, *8*, 864.
(21) Yan, H.; Nykanen, A.; Ruokolainen, J.; Farrar, D.; Gough, J. E.; Saiani, A.; Miller, A. F. Thermo-reversible protein fibrillar hydrogels as cell scaffolds. *Faraday Discuss.* **2008**, *139*, 71−84.
(22) van Dalen, M. C. E.; Vaneyck, J.; Semerdzhiev, S. A.; Karperien, M.; Post, J. N.; Claessens, M. Protein Adsorption Enhances Energy Dissipation in Networks of Lysozyme Amyloid Fibrils. *Langmuir* **2021**, *37*, 7349−7355.
(23) Reynolds, N. P.; Charnley, M.; Mezzenga, R.; Hartley, P. G. Engineered lysozyme amyloid fibril networks support cellular growth and spreading. *Biomacromolecules* **2014**, *15*, 599−608.
(24) Corrigan, A. M.; Donald, A. M. Particle tracking microrheology of gel-forming amyloid fibril networks. *Eur. Phys. J. E* **2009**, *28*, 457−462.
(25) Chaudhuri, O.; Gu, L.; Klumpers, D.; Darnell, M.; Bencherif, S. A.; Weaver, J. C.; Huebsch, N.; Lee, H.-P.; Lippens, E.; Duda, G. N.; et al. Hydrogels with tunable stress relaxation regulate stem cell fate and activity. *Nat. Mater.* **2016**, *15*, 326−334.
(26) Shimanovich, U.; Efimov, I.; Mason, T. O.; Flagmeier, P.; Buell, A. K.; Gedanken, A.; Linse, S.; Åkerfeldt, K. S.; Dobson, C. M.; Weitz, D. A.; et al. Protein Microgels from Amyloid Fibril Networks. *ACS Nano* **2015**, *9*, 43−51.
(27) Semerdzhiev, S. A.; Dekker, D. R.; Subramaniam, V.; Claessens, M. M. A. E. Self-Assembly of Protein Fibrils into Suprafibrillar Aggregates: Bridging the Nano- and Mesoscale. *ACS Nano* **2014**, *8*, 5543−5551.
(28) Nyström, G.; Fong, W.-K.; Mezzenga, R. Ice-Templated and Cross-Linked Amyloid Fibril Aerogel Scaffolds for Cell Growth. *Biomacromolecules* **2017**, *18*, 2858−2865.
(29) Xuan, Q.; Wang, Y.; Chen, C.; Wang, P. Rational Biological Interface Engineering: Amyloidal Supramolecular Microstructure-Inspired Hydrogel. *Front. Bioeng. Biotechnol.* **2021**, *9*, No. 718883.
(30) Jacob, R. S.; Ghosh, D.; Singh, P. K.; Basu, S. K.; Jha, N. N.; Das, S.; Sukul, P. K.; Patil, S.; Sathaye, S.; Kumar, A.; et al. Self healing hydrogels composed of amyloid nano fibrils for cell culture and stem cell differentiation. *Biomaterials* **2015**, *54*, 97−105.
(31) Li, C.; Born, A. K.; Schweizer, T.; Zenobi-Wong, M.; Cerruti, M.; Mezzenga, R. Amyloid-hydroxyapatite bone biomimetic composites. *Adv. Mater.* **2014**, *26*, 3207−3212.
(32) Wegmann, S.; Medalsy, I. D.; Mandelkow, E.; Müller, D. J. The fuzzy coat of pathological human Tau fibrils is a two-layered polyelectrolyte brush. *Proc. Natl. Acad. Sci. U. S. A.* **2013**, *110*, E313−E321.
(33) Klockars, M.; Pettersson, T. Lysozyme concentrations in synovial fluid, pleural fluid and thoracic duct lymph in rheumatoid arthritis. *Scand. J. Rheumatol.* **1985**, *14*, 69−75.
(34) Sidhu, A.; Segers-Nolten, I.; Raussens, V.; Claessens, M. M.; Subramaniam, V. Distinct Mechanisms Determine α-Synuclein Fibril Morphology during Growth and Maturation. *ACS Chem. Neurosci.* **2017**, *8*, 538−547.
(35) Shvadchak, V. V.; Claessens, M. M.; Subramaniam, V. Fibril breaking accelerates α-synuclein fibrillization. *J. Phys. Chem. B* **2015**, *119*, 1912−1918.
(36) Akkermans, C.; Venema, P.; van der Goot, A. J.; Gruppen, H.; Bakx, E. J.; Boom, R. M.; van der Linden, E. Peptides are Building Blocks of Heat-Induced Fibrillar Protein Aggregates of β-Lactoglobulin Formed at pH 2. *Biomacromolecules* **2008**, *9*, 1474−1479.
(37) Fitzpatrick, A. W. P.; Debelouchina, G. T.; Bayro, M. J.; Clare, D. K.; Caporini, M. A.; Bajaj, V. S.; Jaroniec, C. P.; Wang, L.; Ladizhansky, V.; Müller, S. A.; et al. Atomic structure and hierarchical assembly of a cross-β amyloid fibril. *Proc. Natl. Acad. Sci. U. S. A.* **2013**, *110*, 5468−5473.
(38) Ridgley, D. M.; Barone, J. R. Evolution of the amyloid fiber over multiple length scales. *ACS Nano* **2013**, *7*, 1006−1015.
(39) Pieri, L.; Madiona, K.; Bousset, L.; Melki, R. Fibrillar α-synuclein and huntingtin exon 1 assemblies are toxic to the cells. *Biophys. J.* **2012**, *102*, 2894−2905.
(40) Mazaheri, M.; Moosavi-Movahedi, A. A.; Saboury, A. A.; Khodagholi, F.; Shaerzadeh, F.; Sheibani, N. Curcumin Protects β-Lactoglobulin Fibril Formation and Fibril-Induced Neurotoxicity in PC12Cells. *PLoS One* **2015**, *10*, e0133206−e0133206.
(41) Gharibyan, A. L.; Zamotin, V.; Yanamandra, K.; Moskaleva, O. S.; Margulis, B. A.; Kostanyan, I. A.; Morozova-Roche, L. A. Lysozyme Amyloid Oligomers and Fibrils Induce Cellular Death via Different Apoptotic/Necrotic Pathways. *J. Mol. Biol.* **2007**, *365*, 1337−1349.
(42) Harte, N. P.; Klyubin, I.; McCarthy, E. K.; Min, S.; Garrahy, S. A.; Xie, Y.; Davey, G. P.; Boland, J. J.; Rowan, M. J.; Mok, K. H. Amyloid Oligomers and Mature Fibrils Prepared from an Innocuous Protein Cause Diverging Cellular Death Mechanisms. *J. Biol. Chem.* **2015**, *290*, 28343−28352.
(43) Lin, Z.; Fitzgerald, J. B.; Xu, J.; Willers, C.; Wood, D.; Grodzinsky, A. J.; Zheng, M. H. Gene expression profiles of human chondrocytes during passaged monolayer cultivation. *J. Orthop. Res.* **2008**, *26*, 1230−1237.
(44) Ma, B.; Leijten, J. C. H.; Wu, L.; Kip, M.; van Blitterswijk, C. A.; Post, J. N.; Karperien, M. Gene expression profiling of dedifferentiated human articular chondrocytes in monolayer culture. *Osteoarthritis and Cartilage* **2013**, *21*, 599−603.
(45) Healy, E.; Dempsey, M.; Lally, C.; Ryan, M. P. Apoptosis and necrosis: Mechanisms of cell death induced by cyclosporine A in a renal proximal tubular cell line. *Kidney Int.* **1998**, *54*, 1955−1966.
(46) Telford, W. G.; King, L. E.; Fraker, P. J. Rapid quantitation of apoptosis in pure and heterogeneous cell populations using flow cytometry. *J. Immunol. Methods* **1994**, *172*, 1−16.
(47) Singh, P.; Marcu, K. B.; Goldring, M. B.; Otero, M. Phenotypic instability of chondrocytes in osteoarthritis: on a path to hypertrophy. *Ann. N. Y. Acad. Sci.* **2019**, *1442*, 17−34.
(48) Mackie, E. J.; Ahmed, Y. A.; Tatarczuch, L.; Chen, K. S.; Mirams, M. Endochondral ossification: How cartilage is converted into bone in the developing skeleton. *Int. J. Biochem. Cell Biol.* **2008**, *40*, 46−62.
(49) Urist, M. R.; Adams, T. CARTILAGE OR BONE INDUCTION BY ARTICULAR CARTILAGE Observations with Radioisotope Labelling Techniques. *J. Bone Jt. Surg., Br. Vol.* **1968**, *50-B*, 198−215.
(50) Naganuma, T.; Traversa, E. The effect of cerium valence states at cerium oxide nanoparticle surfaces on cell proliferation. *Biomaterials* **2014**, *35*, 4441−4453.
(51) Faucheux, N.; Schweiss, R.; Lützow, K.; Werner, C.; Groth, T. Self-assembled monolayers with different terminating groups as model substrates for cell adhesion studies. *Biomaterials* **2004**, *25*, 2721−2730.
(52) Qiu, Q.; Sayer, M.; Kawaja, M.; Shen, X.; Davies, J. E. Attachment, morphology, and protein expression of rat marrow stromal cells cultured on charged substrate surfaces. *J. Biomed. Mater. Res.* **1998**, *42*, 117−127.
(53) Zhang, X.; Meng, L.; Lu, Q. Cell Behaviors on Polysaccharide-Wrapped Single-Wall Carbon Nanotubes: A Quantitative Study of the Surface Properties of Biomimetic Nanofibrous Scaffolds. *ACS Nano* **2009**, *3*, 3200−3206.

https://doi.org/10.1021/acsomega.3c00151
ACS Omega XXXX, XXX, XXX−XXX

(54) Mendonça, G.; Mendonça, D. B. S.; Aragão, F. J. L.; Cooper, L. F. Advancing dental implant surface technology - From micron- to nanotopography. *Biomaterials* **2008**, *29*, 3822−3835.
(55) Le, B. Q.; Vasilevich, A.; Vermeulen, S.; Hulshof, F.; Stamatialis, D. F.; van Blitterswijk, C. A.; de Boer, J. Micro-Topographies Promote Late Chondrogenic Differentiation Markers in the ATDC5 Cell Line. *Tissue Eng., Part A* **2017**, *23*, 458−469.
(56) Nikkhah, M.; Edalat, F.; Manoucheri, S.; Khademhosseini, A. Engineering microscale topographies to control the cell-substrate interface. *Biomaterials* **2012**, *33*, 5230−5246.
(57) Wu, Y. N.; Law, J. B.; He, A. Y.; Low, H. Y.; Hui, J. H.; Lim, C. T.; Yang, Z.; Lee, E. H. Substrate topography determines the fate of chondrogenesis from human mesenchymal stem cells resulting in specific cartilage phenotype formation. *Nanomedicine* **2014**, *10*, 1507−1516.
(58) de Melo, B. A. G.; Jodat, Y. A.; Mehrotra, S.; Calabrese, M. A.; Kamperman, T.; Mandal, B. B.; Santana, M. H. A.; Alsberg, E.; Leijten, J.; Shin, S. R. 3D Printed Cartilage-Like Tissue Constructs with Spatially Controlled Mechanical Properties. *Adv. Funct. Mater.* **2019**, *29*, 1906330.
(59) Engler, A. J.; Sen, S.; Sweeney, H. L.; Discher, D. E. Matrix elasticity directs stem cell lineage specification. *Cell* **2006**, *126*, 677−689.
(60) Charrier, E. E.; Pogoda, K.; Wells, R. G.; Janmey, P. A. Control of cell morphology and differentiation by substrates with independently tunable elasticity and viscous dissipation. *Nat. Commun.* **2018**, *9*, 449.
(61) Gelderloos, C. C. *Amyloids: from molecular structure to mechanical properties*. VU Amsterdam: Amsterdam, Netherlands, 2014. https://research.vu.nl/en/publications/amyloids-from-molecular-structure-to-mechanical-properties.
(62) Gale, M.; Pollanen, M. S.; Markiewicz, P.; Goh, M. C. Sequential assembly of collagen revealed by atomic force microscopy. *Biophys. J.* **1995**, *68*, 2124−2128.
(63) Shattuck, M. B.; Gustafsson, M. G. L.; Fisher, K. A.; Yanagimoti, K. C.; Veis, A.; Bhatnagar, R. S.; Clarke, J. Monomeric collagen imaged by cryogenic force microscopy. *J. Microsc.* **1994**, *174*, RP1−RP2.
(64) Solomonov, I.; Zehorai, E.; Talmi-Frank, D.; Wolf, S. G.; Shainskaya, A.; Zhuravlev, A.; Kartvelishvily, E.; Visse, R.; Levin, Y.; Kampf, N.; et al. Distinct biological events generated by ECM proteolysis by two homologous collagenases. *Proc. Natl. Acad. Sci.* **2016**, *113*, 10884−10889.
(65) Raspanti, M.; Viola, M.; Sonaggere, M.; Tira, M. E.; Tenni, R. Collagen Fibril Structure Is Affected by Collagen Concentration and Decorin. *Biomacromolecules* **2007**, *8*, 2087−2091.
(66) Pratta, M. A.; Yao, W.; Decicco, C.; Tortorella, M. D.; Liu, R.-Q.; Copeland, R. A.; Magolda, R.; Newton, R. C.; Trzaskos, J. M.; Arner, E. C. Aggrecan Protects Cartilage Collagen from Proteolytic Cleavage. *J. Biol. Chem.* **2003**, *278*, 45539−45545.
(67) Archer, C. W.; Francis-West, P. The chondrocyte. *Int. J. Biochem. Cell Biol.* **2003**, *35*, 401−404.
(68) Meyer, J.; Salamon, A.; Mispagel, S.; Kamp, G.; Peters, K. Energy metabolic capacities of human adipose-derived mesenchymal stromal cells in vitro and their adaptations in osteogenic and adipogenic differentiation. *Exp. Cell Res.* **2018**, *370*, 632−642.
(69) Fu, Y.; Both, S. K.; Plass, J. R. M.; Dijkstra, P. J.; Zoetebier, B.; Karperien, M. Injectable Cell-Laden Polysaccharide Hydrogels: In Vivo Evaluation of Cartilage Regeneration. *Polymer* **2022**, *14*, 4292.
(70) Tan, H.; Marra, K. G. Injectable, Biodegradable Hydrogels for Tissue Engineering Applications. *Materials* **2010**, *3*, 1746−1767.
(71) Jin, R.; Moreira Teixeira, L. S.; Dijkstra, P. J.; van Blitterswijk, C. A.; Karperien, M.; Feijen, J. Chondrogenesis in injectable enzymatically crosslinked heparin/dextran hydrogels. *J. Controlled Release* **2011**, *152*, 186−195.
(72) Moreira Teixeira, L. S.; Bijl, S.; Pully, V. V.; Otto, C.; Jin, R.; Feijen, J.; van Blitterswijk, C. A.; Dijkstra, P. J.; Karperien, M. Self-attaching and cell-attracting in-situ forming dextran-tyramine conjugates hydrogels for arthroscopic cartilage repair. *Biomaterials* **2012**, *33*, 3164−3174.
(73) Zoetebier, B.; Schmitz, T. C.; Ito, K.; Karperien, M.; Tryfonidou, M. A.; Paez, J. I. Injectable Hydrogels for Articular Cartilage and Nucleus Pulposus Repair: Status Quo and Prospects. *Tissue Eng., Part A* **2022**, *28*, 478−499.
(74) Trial, H. C. B. C. *Advanced Cartilage Treatment With Injectable-hydrogel Validation of the Effect (ACTIVE)*. NIH, 2022. https://clinicaltrials.gov/ct2/show/NCT05186935 (accessed 2023 20230321).
(75) Araki, K.; Yagi, N.; Aoyama, K.; Choong, C.-J.; Hayakawa, H.; Fujimura, H.; Nagai, Y.; Goto, Y.; Mochizuki, H. Parkinson's disease is a type of amyloidosis featuring accumulation of amyloid fibrils of α-synuclein. *Proc. Natl. Acad. Sci.* **2019**, *116*, 17963−17969.
(76) Sidhu, A.; Segers-Nolten, I.; Subramaniam, V. Solution conditions define morphological homogeneity of alpha-synuclein fibrils. *Biochim. Biophys. Acta* **2014**, *1844*, 2127−2134.
(77) Gosal, W. S.; Clark, A. H.; Ross-Murphy, S. B. Fibrillar β-Lactoglobulin Gels: Part 1. Fibril Formation and Structure. *Biomacromolecules* **2004**, *5*, 2408−2419.
(78) Arnaudov, L. N.; de Vries, R. Thermally Induced Fibrillar Aggregation of Hen Egg White Lysozyme. *Biophys. J.* **2005**, *88*, 515−526.
(79) Mossuto, M. F.; Dhulesia, A.; Devlin, G.; Frare, E.; Kumita, J. R.; de Laureto, P. P.; Dumoulin, M.; Fontana, A.; Dobson, C. M.; Salvatella, X. The Non-Core Regions of Human Lysozyme Amyloid Fibrils Influence Cytotoxicity. *J. Mol. Biol.* **2010**, *402*, 783−796.
(80) Pace, C. N.; Vajdos, F.; Fee, L.; Grimsley, G.; Gray, T. How to measure and predict the molar absorption coefficient of a protein. *Protein Sci.* **1995**, *4*, 2411−2423.
(81) Schindelin, J.; Arganda-Carreras, I.; Frise, E.; Kaynig, V.; Longair, M.; Pietzsch, T.; Preibisch, S.; Rueden, C.; Saalfeld, S.; Schmid, B.; et al. Fiji: An open-source platform for biological-image analysis. *Nat. Methods* **2012**, *9*, 676−682.
(82) Ye, J.; Coulouris, G.; Zaretskaya, I.; Cutcutache, I.; Rozen, S.; Madden, T. L. Primer-BLAST: A tool to design target-specific primers for polymerase chain reaction. *BMC Bioinf.* **2012**, *13*, 134−111.
(83) Livak, K. J.; Schmittgen, T. D. Analysis of Relative Gene Expression Data Using Real-Time Quantitative PCR and the 2^(ΔΔC_T) Method. *Methods* **2001**, *25*, 402−408.

https://doi.org/10.1021/acsomega.3c00151
ACS Omega XXXX, XXX, XXX−XXX